10. Analysis of Crystallite Orientation

10.1 Crystallite Orientation and the X-Ray Diffraction Diagram

Figure 10.1 shows a schematic illustration of the structural changes of a high polymer specimen by drawing, according to the fringed-micelle model (*cf.* Section 7.2.2.A), and the corresponding X-ray diffraction diagrams obtained from three different directions, mutually orthogonal two directions perpendicular to the drawing direction and the direction parallel

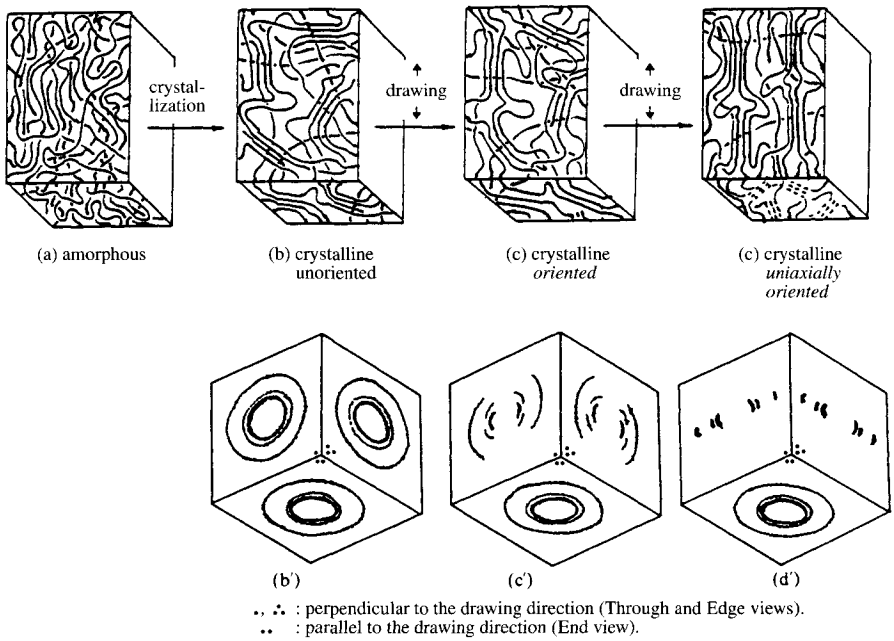

Fig. 10.1 Schematic illustration of structural changes by crystallization and by drawing for a linear high polymer specimen (according to the fringed-micelle model) and the corresponding X-ray diffraction diagrams.

to the drawing direction. An example of X-ray diffraction diagrams obtained for a drawn Nylon 12 specimen from the three directions is given in Fig. 10.2.[1] By drawing or by other mechanical treatments, the central diffuse small-angle scattering taken from the directions mentioned above also show different diagrams corresponding to the different wide-angle diffraction diagrams. An example of a doubly oriented poly(ethylene terephthalate) specimen is given in Fig. 15.36. Fig. 10.3 depicts a schematic illustration of structural change in the metal wire by drawing from a random orientation to a uniaxial orientation. By drawing the randomly oriented $< 111 >$ axis of each cubic unit cell has become parallel to the draw direction.[2] This chapter deals with the preferred orientation of crystallites in high polymer substances. We can easily apply this method to determine the preferred orientation of other substances included in high polymer specimens, such as the preferred orientation of platelet

crystals of $Mg(OH)_2$ in a rolled rubber sheet. The preferred orientation of molecular chains in the amorphous state will be discussed briefly in Section 14.5.

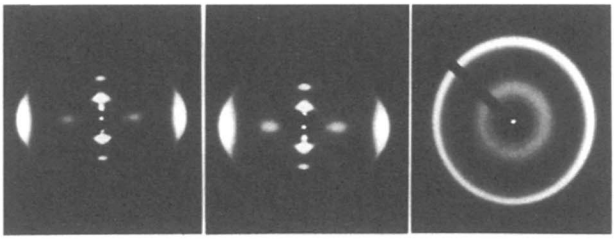

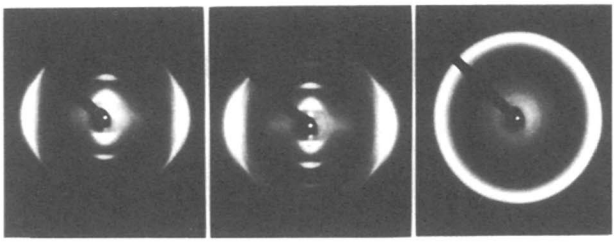

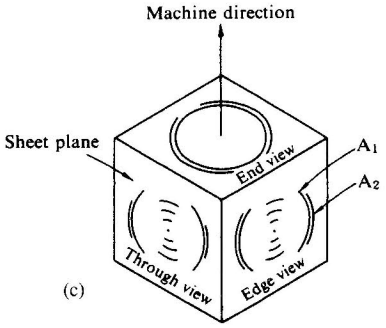

Fig. 10.2 X-ray diffraction diagrams of a drawn Nylon 12 specimen taken from three different directions.[1)]
(a) drawn out uniaxially to 3.0 times from its original length at 100°C (A_1 and A_2 not split).
(b) as above at 160°C (A_1 and A_2 split).
(c) schematic representation of (b).
[Reproduced with permission from T. Ishikawa *et al.*, *J. Chem. Soc. Jpn., Chem. Industrial Chem.*, p. 103, Chem. Soc. Jpn. (1978)]

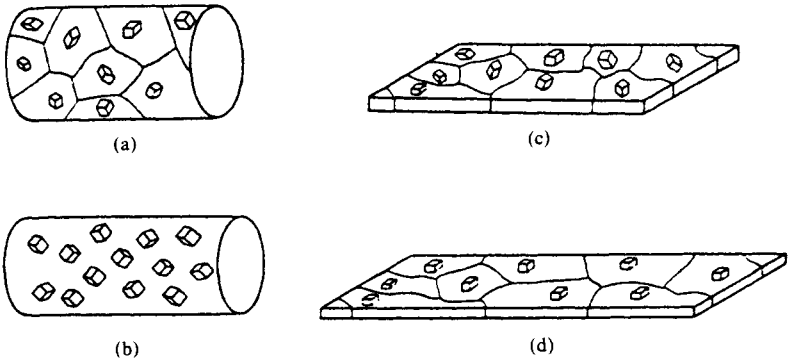

Fig. 10.3 Schematic illustration of preferred orientation in metal wire by drawing.[2]
(a) Random orientation in a cylindrical specimen.
(b)< 111 > Axis of each crystallite (represented by a cubic unit cell) is parallel to the draw direction (horizontal direction).
(c) Random orientation in a plate specimen.
(d) (100) plane of each crystallite is parallel to the plane of the specimen.
[Reproduced with permission from T. Imura, *X-Ray Diffraction* (K. Kohra ed.), p. 600, Kyoritsu Pub. (1980)]

10.1.1 General survey

In a well-oriented specimen, the crystallites or crystalline regions† are generally aligned in such a way that, say, all the c axes lie in the same direction, while the directions of the other two axes are uniformly distributed around the c axis direction. Moreover all the directions of the c axes are uniformly inclined at a constant angle φ to a reference axis (*e.g.* draw direction), OZ in the specimen (*cf.* Fig. 10.4, p. 242).

Let a point O in the specimen be the origin, and let the origins of all the crystallites be transposed to this point. The reciprocal lattice points R of an arbitrary set of planes (hkl) in the crystallites (where OR is inclined at an angle σ to the c axis, at a distance from the origin $OR = r^* = 1/d_{(hkl)}$) trace out a circle (the reciprocal lattice point circle) with the c axes passing through its center, as shown in Fig. 10.4(b). Since the c axes of the crystallites are uniformly distributed around the fixed direction OZ in the specimen at an angle φ to OZ, the small circle traced by the reciprocal lattice points R generates a band (the reciprocal lattice point distribution band) by revolution about OZ as shown in Fig. 10.4(b). There is a corresponding band for the $(\overline{hkl})$ planes, and the two together form a symmetrical arrangement along the Z axis (Fig. 10.4(c)).

If X-rays are incident upon the specimen from (say) the $\overline{Y}$O direction, the reciprocal lattice points on the intersection of the distribution band with the diffraction sphere, *i.e.* on the arc R_1R_2 in Fig. 10.5, give rise to diffraction. A diffraction arc P_1P_2, corresponding to the arc R_1R_2, will now appear on a flat film placed normal to the incident X-rays. Due to the symmetrical arrangement of the reciprocal lattice distribution bands along the X and Z axes, the result will be four diffraction arcs arranged symmetrically with respect to the ξ and ζ axes on the film.

In Fig. 10.4(b), the distribution of the reciprocal lattice point R around the c axis is constant, but as this axis itself revolves, the density distribution on the reciprocal lattice point

† "Crystallite" will be used throughout this chapter to indicate "crystallite", "crystalline region" or "crystalline part."

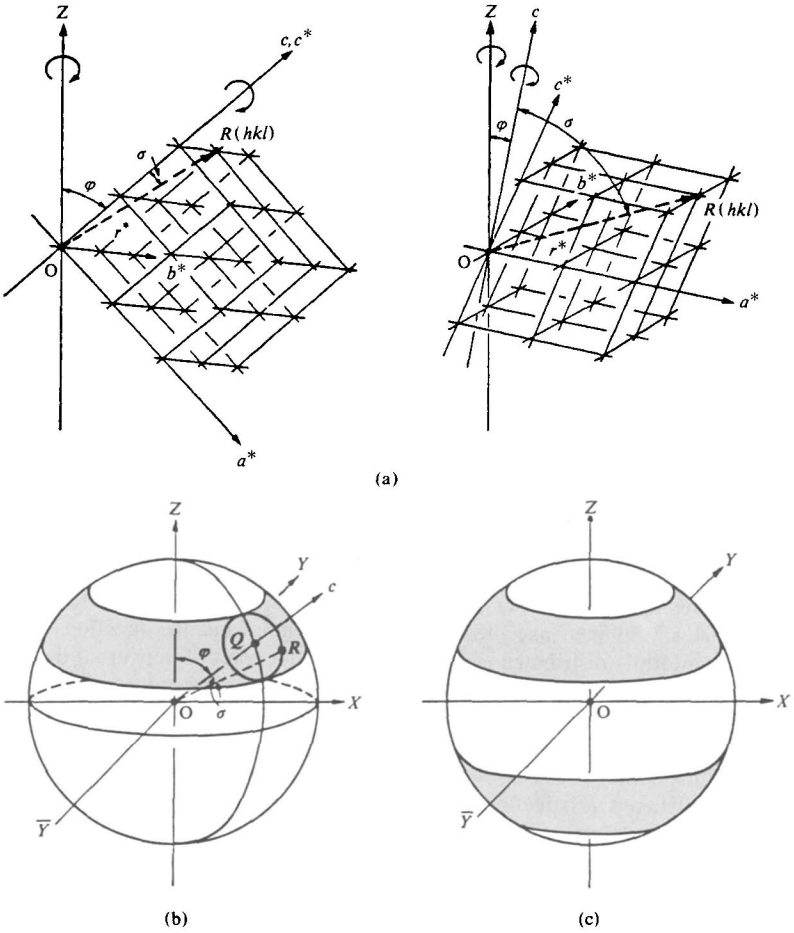

Fig. 10.4 Crystallite orientation, the reciprocal lattice, and the reciprocal lattice point distribution bands.
(a) Reciprocal lattice orientation corresponding to the orientation of the crystallites. Left: orthorhombic; right: triclinic system.
(b) Distribution band for an arbitrary reciprocal lattice point R.
(c) Symmetrical arrangement of the distribution bands about the Z axis.

distribution band is at its densest along the upper and lower edges of the band, and is least along the path of the center Q. The intensity distribution along the diffraction arc P_1P_2 is accordingly greatest at its ends and least in the center (Fig. 10.5(b)). The two ends of the diffraction arc P_1P_2 are located by the following relationships (*cf.* Fig. 10.5(a)):

$$\cos \delta_1 = \cos(\varphi - \sigma)/\cos \theta, \qquad \cos \delta_2 = \cos(\varphi + \sigma)/\cos \theta \tag{10.1}$$

The form of the reciprocal lattice point distribution bands, and hence also of the diffraction patterns, varies with the relationship between φ and σ. The four arcs may be joined in pairs to give two arcs intersecting either the ξ or the ζ axis, or all four may even

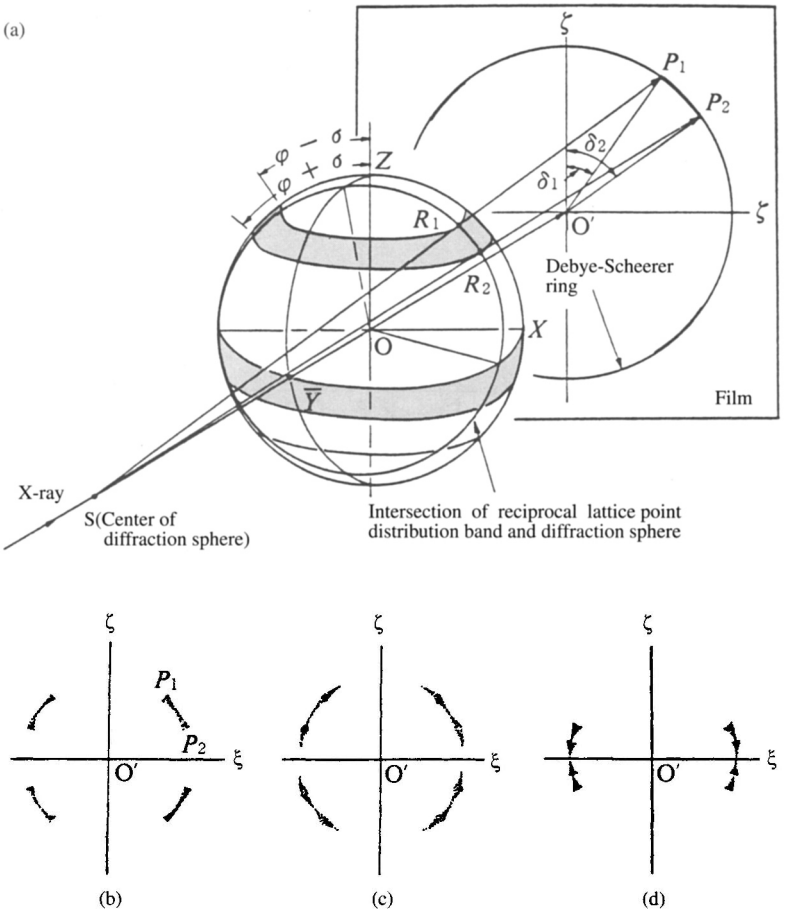

Fig. 10.5 Spiral Orientation.
(a) Geometrical relationship between lattice point distribution and the diffraction pattern.
(b) Form of the diffraction pattern that would be given by an ideally oriented sample.
(c) General form of the diffraction pattern as actually observed.
(d) Form of the diffraction pattern that would be given by an ideally oriented sample where $(\varphi + \sigma) > 90^\circ$ (see Fig. 10.6), *i.e.* where the distribution bands overlap.

be joined to form a complete circle. The principal variants of the forms of the reciprocal lattice point distributions and of the diffraction patterns are shown in Figs. 10.5, 10.6, 10.7, and 10.9. Diffraction patterns for the ideally oriented state are shown, together with sketches of those actually observed. In practice, the orientations of the crystallites in a specimen never correspond to a single fixed value of φ. Some crystallites with orientations at different angles will always be present, the number of crystallites inclined at a given angle decreasing as the deviation $\Delta\varphi$ of this angle from φ increases (see Fig. 10.7(b) and(d)). Examples of the kinds of diffraction patterns obtained under these circumstances are also given in Figs. 10.5, 10.7, and 10.9.

10.1.2 Types of orientation

Crystallite orientations are generally classified as uniaxial or biaxial. The uniaxial orientation includes simple fiber structures ($\varphi = 0°$), spiral fiber structures ($0 < \varphi < 90°$), and ring fiber structures ($\varphi = 90°$). Certain special kinds of intermediate orientation are also recognized. The characteristics of various types of orientation are described below.

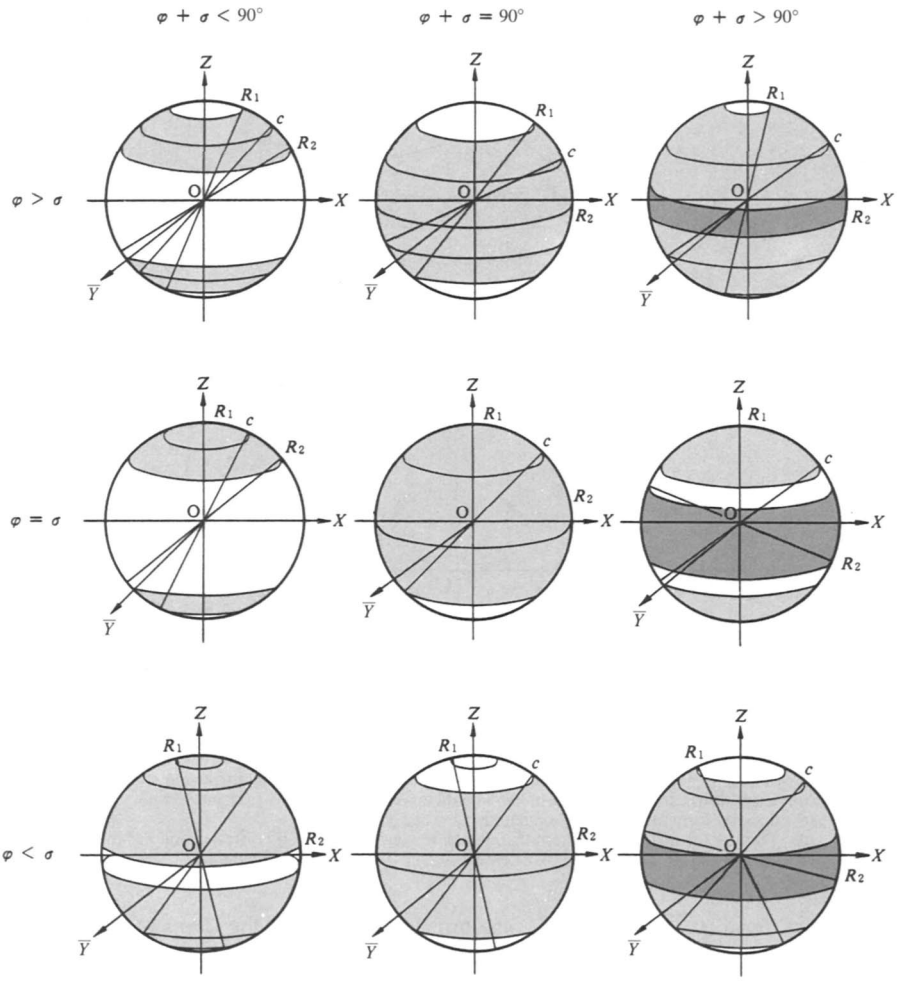

Fig. 10.6 Various forms of reciprocal lattice point distributions for spiral orientation.
As in Figs. 10.4 and 10.5, φ is the helix angle (*i.e.* the inclination of the c axis to the fiber axis) and σ is the angle between the reciprocal lattice vector and the c axis.

A. Uniaxial orientation (simple fiber structure)

Here ($\varphi = 0°$, *i.e.* the c axis coincides with the Z axis (Fig. 10.7). The reciprocal lattice is cylindrically symmetrical with respect to the fiber axis (*cf.* Fig. 4.14(c)), and the X-ray dia-

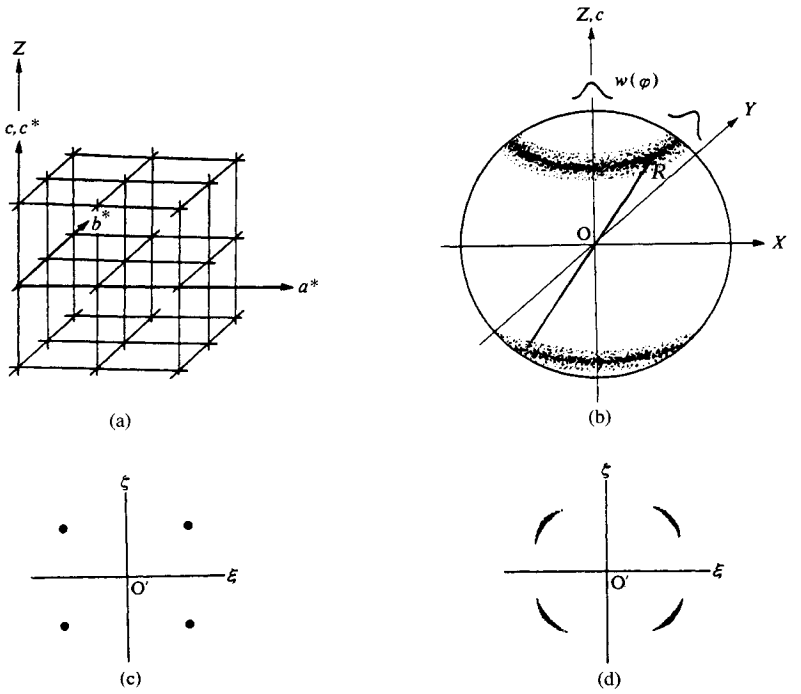

Fig. 10.7 Uniaxial orientation, the reciprocal lattice point distribution, and the resultant diffraction pattern (*cf.* Figs. 4.14, 4.15).
(a) Orientation with respect to the fiber axis Z (ideal case, $\varphi = 0$).
(b) Distribution for a reciprocal lattice point R, showing the effect of small deviations, $w(\varphi)$.
(c) Diffraction from an ideal specimen.
(d) Diffraction from an actual specimen with imperfectly aligned crystallites (*cf.* (b)).

gram obtained with the incident X-rays normal to the fiber axis is essentially the same as a complete rotation photograph for a single crystal (*cf.* Section 4.4.4 and Fig. 10.8). Since $\varphi = 0°$, we find for the general reciprocal lattice point:

$$\delta = \delta_1 = \delta_2, \quad \therefore \cos\delta = \cos\sigma/\cos\theta \tag{10.2}$$

and a four-point diagram is obtained instead of a four-arc diagram. If the incident X-rays are parallel to the fiber axis, on the other hand, the diffraction pattern made for this direction is as if the specimen were unoriented, forming a complete circle (*i.e.* a Debye-Scherrer ring see Fig. 10.1(c')and (d')).

B. Spiral orientation (spiral fiber structure)

Spiral fiber structure is the most general case, $0° < \varphi < 90°$, and all that appears in connection with Fig. 10.4 to 10.6 (above) applies to this category of structures.

C. Ring orientation (ring fiber structure)

Here $\varphi = 90°$, and Eq. 10.1 gives, therefore,

$$\cos\delta_1 = \sin\sigma/\cos\theta = -\cos\delta_2 \quad \therefore \delta_2 = 180° - \delta_1 \tag{10.3}$$

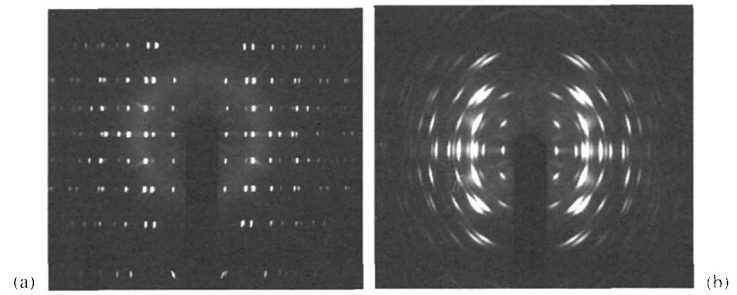

Fig. 10.8 X-ray diffraction patterns of a polyethylene oxide-urea complex.
(a) Single crystal rotation photograph (rotation about the c axis).
(b) Fiber diagram of complex prepared by immersing *uniaxially oriented* polyethylene oxide in urea. The similarity with (a) is evident. [Reproduced with permission from H. Tadokoro *et al.*, *J. Polym. Sci.*, **B2**, 363, John Wiley & Sons, Inc. (1964)]

When the incident X-rays are normal to the X axis, this type of structure always gives two arcs or spots intersecting the equator and extending symmetrically above and below the equator (Fig. 10.9).

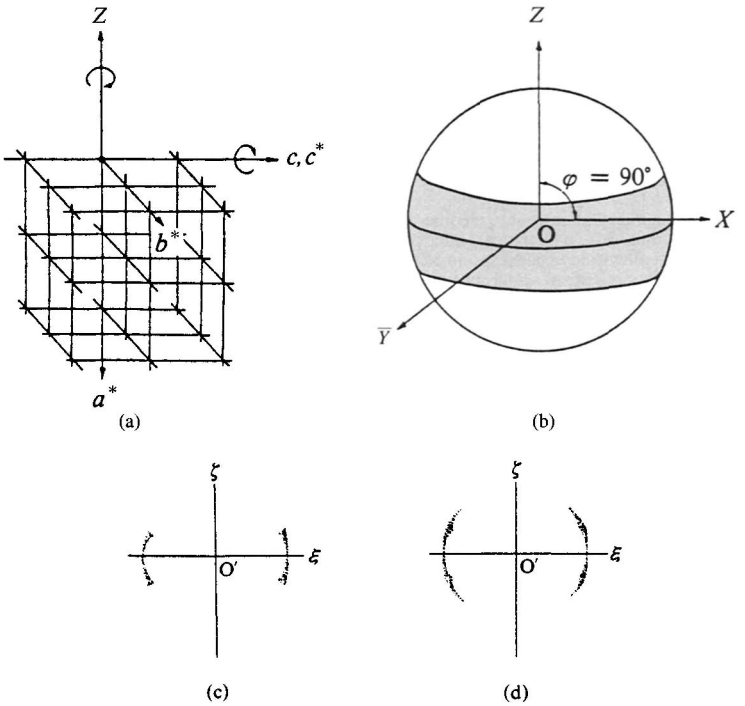

Fig. 10.9 Ring orientation, the reciprocal lattice point distribution, and the resultant diffraction pattern.
(a) Orientation with respect to the fibre axis Z (ideal case, $\varphi = 90°$).
(b) Distribution for a reciprocal lattice point.
(c) Diffraction from an ideal specimen.
(d) Diffraction from an actual specimen.

If the incident X-rays are in the Z direction, however, the diffraction sphere and the reciprocal lattice point distribution band are parallel. Thus, when the diffraction sphere intersects the distribution band, a circle of uniform intensity is produced. The diffraction diagram is therefore of the same form as that given by an unoriented specimen. To distinguish between an unoriented structure and a ring-oriented structure in such cases, the specimen is inclined (*cf.* Section 10.1.3). The diffraction diagram of an unoriented specimen will be unchanged, whereas a change to two arcs intersecting the equator indicates ring orientation.

D. Tilted orientation

In tilted orientation, the crystallite distribution corresponds to a cylindrically symmetrical distribution of the tilted *c* axis, *with no rotation* about the *c* axis. The reciprocal lattice is shown in Fig. 10.10. It is evident that the equatorial line and the layer lines are generally not well developed, and vary with the angle of inclination. The diffraction is observed around the position in which it should appear as a layer line in the case of uniaxial orientation. This corresponds to a rotation photograph for a single crystal with inaccurate alignment of the crystal (a tilted single crystal), and where the axis of rotation corresponds to the fiber axis.

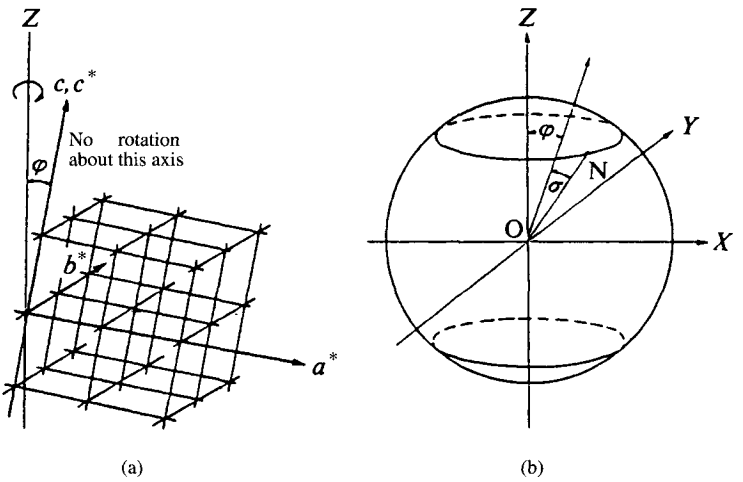

Fig. 10.10 Tilted orientation and the corresponding reciprocal lattice point distribution.
(a) Orientation with respect to the fiber axis Z: $0° < \varphi < 90°$, but this orientation is not to be confused with spiral orientation; there is no rotation about the *c* axis.
(b) Distribution for a reciprocal lattice point *R*. Compare the uniaxial orientation in Fig. 10.7.

E. Biaxial orientation

This type of orientation is the most restrictive one. Like a single crystal of low molecular weight compound mounted on a goniometer head, a crystal axis is oriented parallel to the Z axis (reference axis) and one of the other two axes is also oriented parallel to a reference plane (say) the film plane (for further details see Section 10.3.2.). This type of oriented structure cannot be further ordered except by decreasing the number of crystallites by joining them into larger ones. The fact that a Weissenberg or precession photograph is very similar to that of a single crystal enables ready identification of this type of orientation.

The density distributions of the various reciprocal lattice points can be determined from the intensity distribution of diffractions on a Weissenberg or precession photograph.

F. Double orientation

In this structure, a crystal axis is oriented parallel to the Z axis and a particular crystal plane to lie in the reference plane, the film plane. In many circumstances, there may be two or more different orientations of the unit cell in the specimen; four different orientations are possible for crystals of the monoclinic and triclinic systems (see Fig. 10.11).[3] This type of orientation gives photographs which are like the oscillation photographs of single crystals or twinned crystals (see Fig. 10.8).

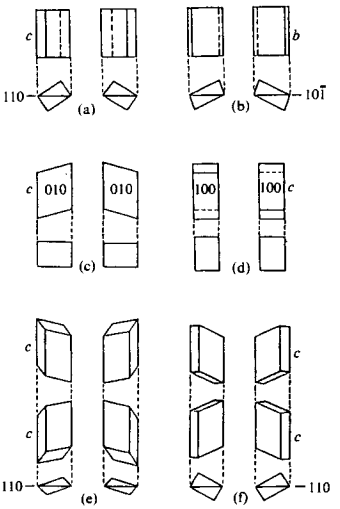

Fig. 10.11 Twinned orientations of unit cell in specimen.[3]
Examples of twins.
(a) Orthorhombic system with fiber axis c, favored plane (110) (or any ($hk0$) where $h, k \neq 0$).
(b) Monoclinic system with fiber axis b, favored plane (101) (or any ($h0l$) including (100) and (001)).
(c) Monoclinic system with fiber axis c, favored plane (010).
(d) As in (c), but favored plane (100).
Examples of quadruplets.
(e) Triclinic system with fiber axis c, favored plane (110) (or any ($hk0$), including (100) and (010)).
(f) Monoclinic system with fiber axis c, favored plane (110) (or any ($hk0$) where $h, k \neq 0$).
[Reproduced from C. W. Bunn, *Chemical Crystallography*, p. 179, The Clarendon Press (1945)]

10.1.3 Interpretation of inclined X-ray diagrams

These are the diffraction diagrams obtained when the incident X-rays are inclined at an oblique angle with respect to the Z axis. The locus of the reciprocal lattice point distribution is unchanged. However, since the diffraction sphere is inclined as shown in Fig. 10.12(a) (angle of inclination $= \mu$), the top two of the four arcs are situated closer together, while the bottom two are farther apart.

If the angular displacements of the ends of the upper and lower arcs from the ζ axis are δ_1, δ_2, δ_3, and δ_4, we obtain relationships of the type (*cf.* Fig. 10.12 (b))

$$\left.\begin{aligned}\cos\delta_1 &= \{\cos(\varphi-\sigma)+\sin\mu\sin\theta\}/\cos\mu\cos\theta\\ \cos\delta_2 &= \{\cos(\varphi+\sigma)+\sin\mu\sin\theta\}/\cos\mu\cos\theta\end{aligned}\right\} \tag{10.4}$$

$$\left.\begin{aligned}\cos\delta_3 &= \{-\cos(\varphi+\sigma)+\sin\mu\sin\theta\}/\cos\mu\cos\theta\\ \cos\delta_4 &= \{-\cos(\varphi-\sigma)+\sin\mu\sin\theta\}/\cos\mu\cos\theta\end{aligned}\right\} \tag{10.5}$$

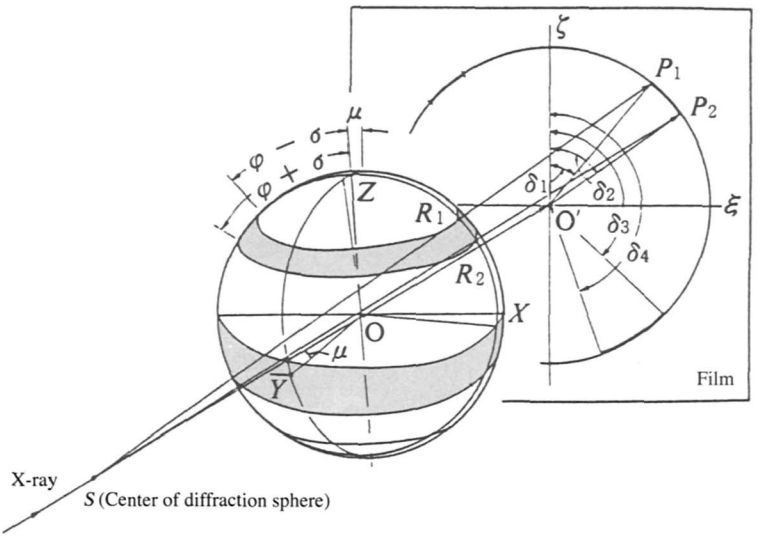

(a)

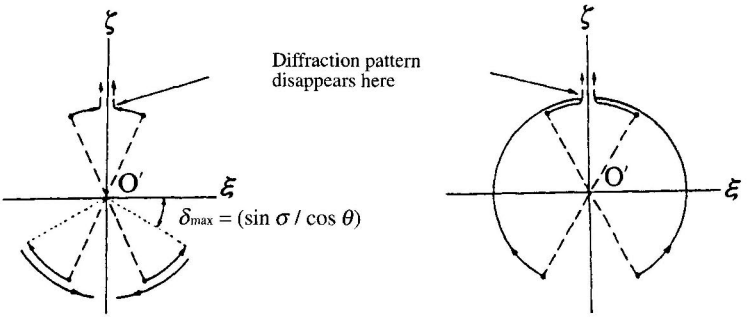

(b)

Reciprocal lattice point sphere
smaller than diffraction sphere
$\sigma < (90^\circ - \theta)$

Reciprocal lattice point sphere
larger than diffraction sphere
$\sigma > (90^\circ - \theta)$

Fig. 10.12 The effect of oblique X-ray incidence upon the diffraction pattern.
(a) Geometry of the reciprocal lattice point distribution and the diffraction pattern.
(b) Variation of the diffraction pattern with inclination angle, μ of X-ray incidence. The arrows indicate movement of the diffraction elements.

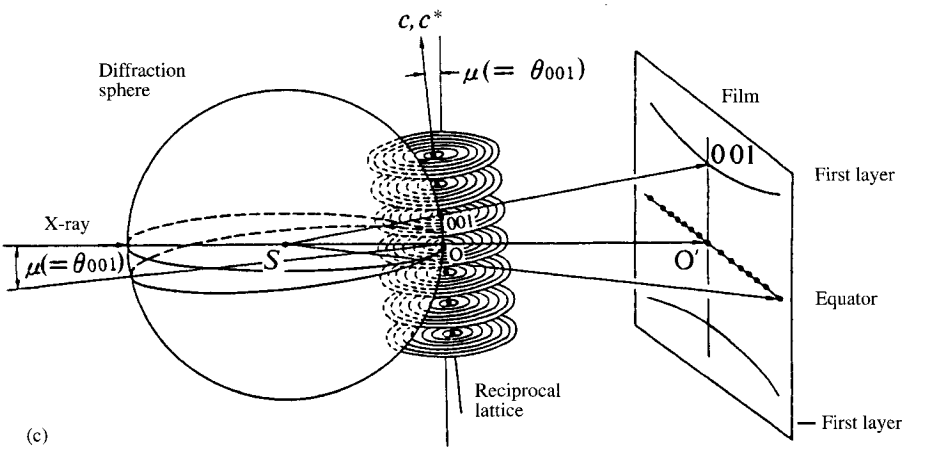

Fig. 10.12 — *Continued*
(c) Ideal case for uniaxial orientation (*cf.* Fig. 4.14(d))

For uniaxial orientation, since $\varphi = 0$, we obtain

$$\left.\begin{aligned}\cos\delta_U = \cos\delta_1 = \cos\delta_2 = \{\cos\sigma + \sin\mu\sin\theta)/\cos\mu\cos\theta\\ \cos\delta_D = \cos\delta_3 = \cos\delta_4 = \{-\cos\sigma + \sin\mu\sin\theta)/\cos\mu\cos\theta\end{aligned}\right\} \quad (10.6)$$

where δ_U and δ_D are the upward and downward displacements respectively.

If the angle of inclination μ of the incident X-rays in Fig. 10.12(a) is gradually increased, the positions at which the diffraction sphere cuts the reciprocal lattice point distribution band in the upper half of the sphere move closer together, and the lengths of the intersections increase, until the two intersections merge into one. The changes in the positions of the diffraction arcs on either side of the meridian with μ are shown in Fig. 10.12(c).

Inclined X-ray diagrams are very useful for measurements of the 00l diffractions, which do not appear with a normal incident beam. However, for the reasons given above, non-meridional diffractions which appear near the 00*l* diffractions merge to give a single-arc diffraction pattern on the meridian (see also Section 10.3.1A).

10.2 Analysis of the Type of Crystallite Orientation

10.2.1 Establishing the presence or absence of orientation

This is established by inspection of the X-ray diffraction photographs of the specimen. It follows from the relationship between the form of the reciprocal lattice point distribution band and the diffraction pattern (established in Figs. 10.4 to 10.9) that diffractions in the form of points or arcs, *i.e.* rings with non-uniform intensity distributions, indicate the presence of orientation. The presence of orientation may also be assumed if, even when Debye-Scherrer rings of uniform intensity are obtained, certain of the rather intense diffractions that would be expected from an unoriented specimen are missing; there is a strong possibility that uniaxial or ring orientation is responsible in this case (*cf.* Section 10.1). If a single X-ray diffraction photograph does not indicate the presence of orientation, the shapes of the diffraction patterns obtained for various incident directions of the X-rays are examined.

The specimen may safely be assumed to unoriented in the majority of cases if this still fails to produce evidence of orientation. It is advisable, however, to check for the presence of spherulites under (say) a polarizing microscope, particularly for specimens in which spherulites readily develop. It is then finally possible to say whether the uniform intensity distribution of the X-ray diagram is due to averaging of the orientations in all directions caused by the presence of many spherulites small in size relative to the X-ray beam, or whether the specimen is in fact quite unoriented. Section 14.4 deals with the case where oriented diffraction may be masked by amorphous halos.

10.2.2 Identification of the type of orientation

A. Utilizing special features of the X-ray diffraction diagram

Table 10.1 presents various criteria for the determination of the type of orientation in comparatively highly oriented specimens. Using a schedule of this nature, the possible types of orientation may be deduced from the features of the diffraction diagram (*cf.* Figs. 10.4 to 10.9). The next stage is to index the diffraction spots (or arcs), and establish the type of orientation from the reciprocal lattice.

Table 10.1 Criteria for determination of the type of crystallite orientation

1st pattern; X-rays are normal to the specimen axis†	**2nd pattern;** X-rays still normal, but in different direction	**3rd pattern;** X-rays are oblique to the specimen axis	Possible types of orientation
(1) *Layer lines clearly developed*			
Resembles single crystal oscillation/rotation photograph; period in axis direction ≈unit cell edge length	Pattern *differs*, but still resembles oscillation/rotation photograph	→	Biaxial (Double)
	Pattern unchanged	→	Uniaxial
(2) *Layer lines not very clearly developed* Consists of many arcs	Pattern unchanged	→	Tilted / Spiral
(3) *Layer lines unrecognizable*			
Arcs, intensity concentrated at equator	→ Pattern unchanged	→ Rings, each with uniform intensity	→ Ring
or			
Rings, each with uniform intensity	→ Pattern unchanged	→ Arcs, intensity concentrated at equator	→ Ring
		Pattern unchanged	→ Unoriented

† Taken as the direction of rolling or drawing.

If the degree of orientation is low, it may not be possible to determine the type of orientation, even though the presence of some kind of orientation may be evident. In such cases the degree of orientation must be increased by suitable treatment such as drawing or rolling to enable identification of the type.

a) Determination of the helix angle φ for specimens with spiral orientation. The helix angle φ for specimens with spiral orientation, *i.e.* the inclination of the c axis with respect to the fiber axis, is found from the azimuthal angle δ as follows:

1) δ_e is found from the $hk0$ diffractions (the equatorial diffractions). Since $\sigma = 90°$ for the equatorial ($hk0$) planes, Eq. 10.1 gives

$$\cos \delta_1 = \sin \sigma / \cos \theta = -\cos \delta_2 \quad \therefore \quad \delta_2 = -\delta_1$$

The complementary angle δ_e of δ_1 satisfies the following equation

$$\sin \varphi = \sin \delta_e \cos \theta \tag{10.7}$$

Thus (1) $\cos \theta \cong 1$, and $\delta_e \cong \varphi$ when the diffraction angle is small, but (2) δ_e is generally slightly greater than φ.

2) δ_m is found from the $00l$ diffractions (the meridional diffractions). If the a and b axes of the crystallites are both perpendicular to the c axis, $\sigma = 0$ for the $(00l)$ planes, and Eq. 10.1 gives

$$\cos \delta_1 = \cos \varphi / \cos \theta = \cos \delta_2 \quad \therefore \quad \delta_1 = \delta_2$$

Whereas the diffractions from the other crystal planes are all in the form of arcs, those from the $(00l)$ planes are points, and give a four-point diagram.

It we let $\delta_1 = \delta_m$, we obtain

$$\cos \delta_m \cos \theta = \cos \varphi \tag{10.8}$$

Thus (1) $\cos \theta \cong 1$, and $\delta_m \cong \varphi$ when the diffraction angle is small, but (2) δ_m is generally slightly smaller than φ.

3) The average of the measured values of δ_m and δ_d gives a reasonably close approximation to the helix angle φ.

4) If only one of δ_m and δ_d can be found, this may be taken as a measure for φ.

b) Determination of the azimuthal angle δ.

1) When a flat film is used, the azimuthal angle δ can be obtained by direct measurement of the angle between the meridian and the point of maximum intensity of the diffraction arcs (or points) on the film.

2) There are two cases when a cylindrical film is used; (1) the fiber axis may be parallel to the cylinder axis, and (2) the axis may be perpendicular. In 1), with the film unrolled (see Fig. 10.13(a)), the value of Z for the point of maximum intensity is measured, and δ found from Eq. 10.9.

$$\cos \delta = \sin \nu / \sin 2\theta, \quad \tan \nu = z/R_F \tag{10.9}$$

where R_F is the radius of the cylindrical film camera. In the case of 2) the procedure is exactly the same (see Fig. 10.13(b)), with z measured and δ found from Eq. 10.10.

$$\sin \delta = \sin \nu / \sin 2\theta, \quad \tan \nu = z/R_F \tag{10.10}$$

c) Determination of the fiber axis. The fiber axis may be found from the "layer-line conditions." Thus, in a rotation photograph with the fiber axis $[uvw]$ as the rotation axis, if a diffraction having the indices hkl appears in the nth layer line, the following relationship holds.[4)]

$$hu + kv + lw = n \tag{10.11}$$

The fiber axis can therefore be easily found from the layer line in which the hkl diffraction appears, with the aid of Eq. 10.11.

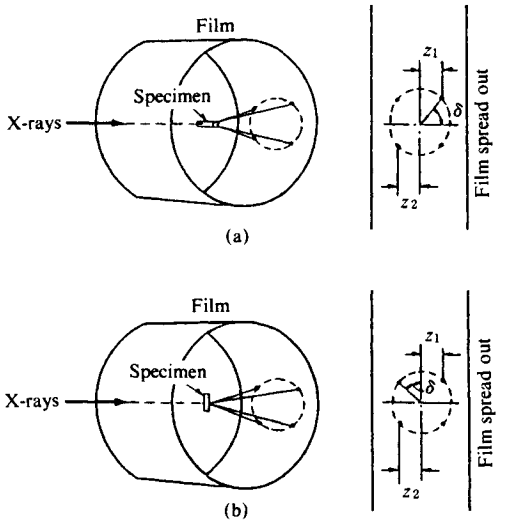

Fig. 10.13 Measurement of the azimuthal angle δ in the case of a cylindrical film.
(a) Fiber axis parallel to the axis of rotation of the camera.
(b) Fiber axis perpendicular to the axis of rotation of the camera Film as unrolled.
[Reproduced with permission from IUCr., *International Tables for X-Ray Crystallography*, (C.H. Mac Gravry, G.D. Rieck eds.), Vol. III, p. 295, IUCr. (1968)]

B. Utilizing the pole figure[5)]

Pole figures are stereographic projections showing the density of crystallographic poles of certain planes as a function of orientation,[6)] and so provide a good method of representing orientation. A pole is the point of intersection of the normal to a crystal plane with the surface of a sphere having the crystal at its center. If the radius of the sphere is $r^* = 1/d_{(hkl)}$, the pole coincides with the reciprocal lattice point of this plane, and the density of the poles on the surface of the sphere is a faithful representation of the reciprocal lattice point density distribution.

If the crystallite orientation is completely random, the poles will be scattered all over the stereographic projection.† If orientation is present, on the other hand, the poles will tend to be concentrated in certain areas within the projection, while the remaining areas will be completely unpopulated.

Figure 10.14 shows pole figures for the (00*l*) planes and those for (*hk*0) planes containing the fiber axis (*c* axis) for various types of orientation. These can be used for comparison with experimental pole figures to determine the type of orientation.

The degree of orientation can also be found from the pole density. The fiber axis can be determined graphically by using a pole figure.[5)]

C. Utilizing small-angle scattering

This heading is included for completeness here, but a full description accompanied by actual examples is deferred until Section 15.4.2.

† For a completely unoriented specimen, the number of poles in a given area on the surface of the projection sphere with the specimen as its center will be constant. Since the stereographic projections is a planar projection of the spherical surface, however, areas are not faithfully reproduced, and the apparent pole distribution even in the pole figure of an unoriented specimen will have a lower concentration near the center.

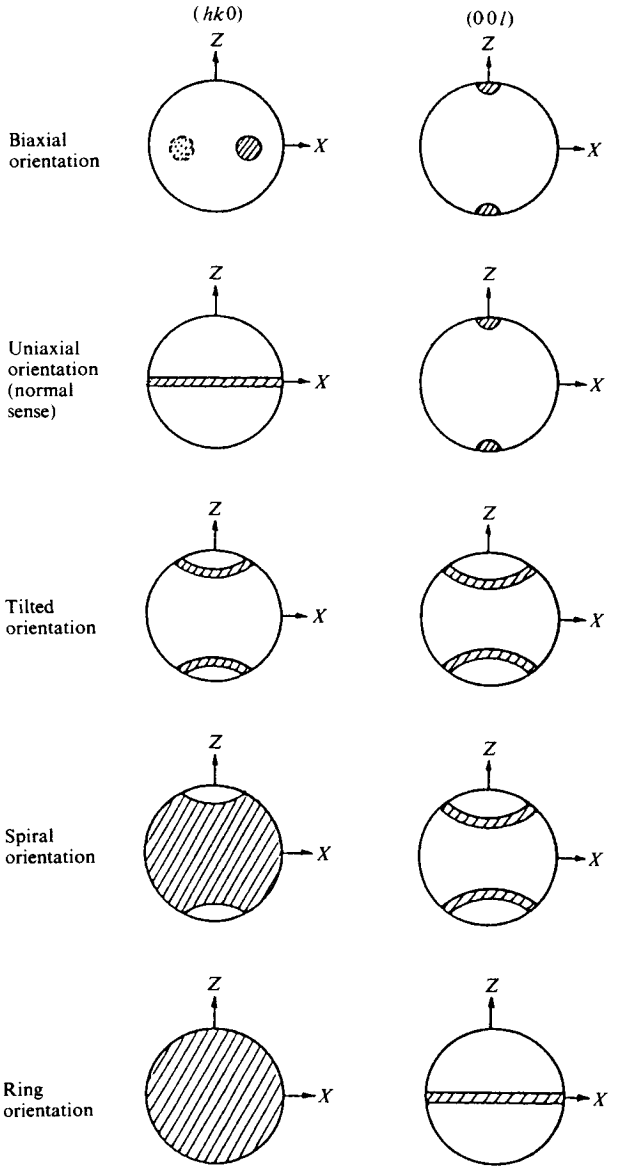

Fig. 10.14 Pole figures for various types of orientation.
The Z direction is taken as parallel to that of drawing or rolling (milling), and in the latter the X direction is parallel to the rolled surface and normal to the rolling direction.
[Reproduced with permission from C.J. Heffelfinger, R.L. Burton, *J. Polym. Sci.*, **47**, 290, John Wiley & Sons, Inc. (1960)]

D. Determination of the type of orientation

The variation of the type of orientation in the necking portions of cold-drawn polyethylene is described in Section 15.4.1 in connection with the results of small-angle scattering analyses. In the present section we shall discuss the analysis of the type of orientation in the interior of spherulites and of the orientation of extruded polyethylene film.

a) Radial variation of the orientation in spherulites. As was mentioned earlier, if the X-ray beam is very large in proportion to the size of the spherulites in the specimen, the orientations in the various regions inside the spherulites average out, and a completely unoriented X-ray diagram may be obtained. If, on the other hand, we use microbeam X-ray diffraction (*cf.* Section 8.2) with a sufficiently small beam in proportion to the size of the spherulites, the X-ray diagram will give evidence of orientation.

Figure 10.15[7] shows a large polyethylene spherulite measuring 0.5 ~ 1 mm. Extinction rings are observed at intervals of about 50 micrometers. As shown in the diagram, the continuous radial variation of the orientation was traced by making X-ray diffraction patterns at intervals of 13 micrometers along a radius, using a microbeam having dimensions of about 2 × 1.3 micrometers. The variations of the 110 and 200 diffractions are shown in Fig. 10.15(b).

The results were analyzed in terms of the reciprocal lattice as follows. Fig. 10.15(c) shows the limited distribution of the reciprocal lattice points for part of the reciprocal lattice of polyethylene. The intersections of the reciprocal lattice points with the diffraction sphere are therefore arcs, and the diffractions are accordingly also arcs rather than spots. Fig. 10.15(d) shows the projection of the reciprocal lattice onto the a^*c^* plane; I, II, III,..., VII identify the successive directions of the Incident X-rays. The shapes of the intersec-

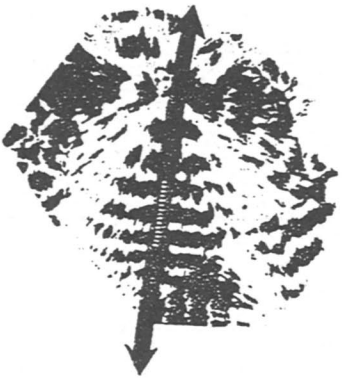

(a)

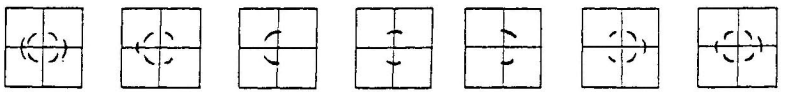

(b) I II III IV V VI VII

Fig. 10.15 Investigation of the orientation in polyethylene spherulites by microbeam X-ray diffraction.[7]
(a) Photomicrograph of the specimen taken in polarized light. The points marked along the superimposed arrow show the positions at which diffractions were obtained.
(b) Sketches of the 110 and 200 diffractions obtained at successive positions.

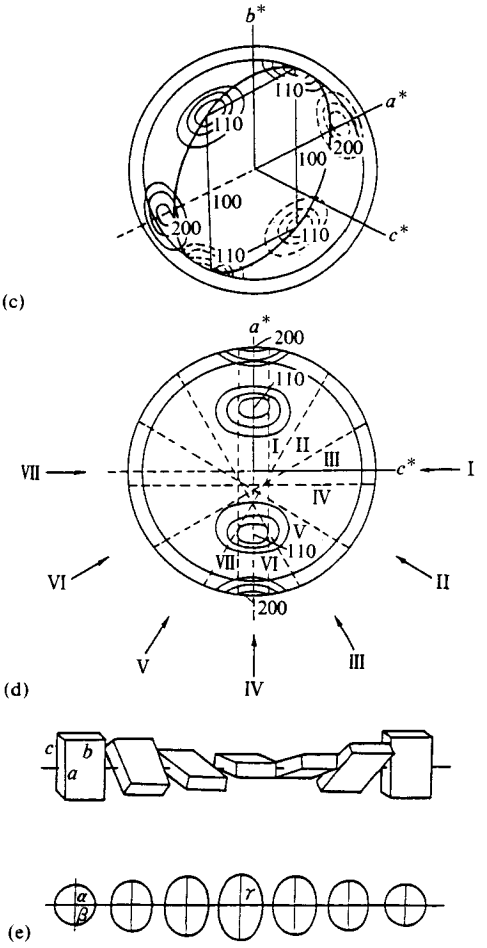

Fig. 10.15 — *Continued*
(c) Part of the reciprocal lattice of polyethylene.
(d) Projection of the reciprocal lattice onto the a^*c^* plane.
I, II,...,VII indicate the directions of the incident X-rays corresponding to the diffractions in (b).
(e) Helical arrangement of unit cells along the radius of the spherulite (upper diagram).
Corresponding rotation of the index ellipsoid with refractive indices α, β, and γ (lower diagram).
[Reproduced with permission from Y. Fujiwara, *J. Appl. Polym. Sci.*, **4**, 11, John Wiley & Sons, Inc. (1960)]

tions of the reciprocal lattice points with the diffraction sphere vary when the diffraction patterns obtained (Fig. 10.15(b)) are interpreted as follows. The b axis is always directed along the radius, while the variation of the 110 intensity shows that the c axis twists as illustrated in Fig. 10.15(e). It is also interesting to note that orientations II and VI in Fig. 10.15(b) are practically identical, and that a rotation through 180° occurs in a distance of $4 \times 13 = 52$ micrometers. The half-period of this twisting of the c axis thus coincides with the spacing of the rings due to double refraction, and a dark ring is observed whenever the c axis is perpendicular to the basal plane.

b) Pole figures of extruded polyethylene film. Figure 10.16 shows the pole figures obtained for the 200, 020, and 002 diffractions from extruded polyethylene (Marlex 50) tubular film.[8)]

It is clear from the (200) pole figures that at a blow ratio of 1.7 : 1, the *a* axis is directed along the extrusion direction, but with maximum concentrations at 45° and at 135° to the plane of the film. This result shows that the *a* axes in the extruded material are not parallel to the extrusion direction, as had been thought, but are oriented at an angle of 45° to this direction. As the blow ratio is increased the *a* axes naturally become parallel to the extrusion direction in accordance with the earlier view.

Examination of the (020) pole figures shows that the *b* axes are distributed in a plane perpendicular to the extrusion direction, and that the degree of orientation is much higher than that of the *a* axes. This is also something that had not previously been established conclusively, since the 020 intensity is much lower than the 200 intensity. Moreover, the direction of orientation of the *b* axes shows practically no change with increasing blow ratio.

The (002) pole figures show that at a blow ratio of 1.7 : 1, the orientation of the *c* axis

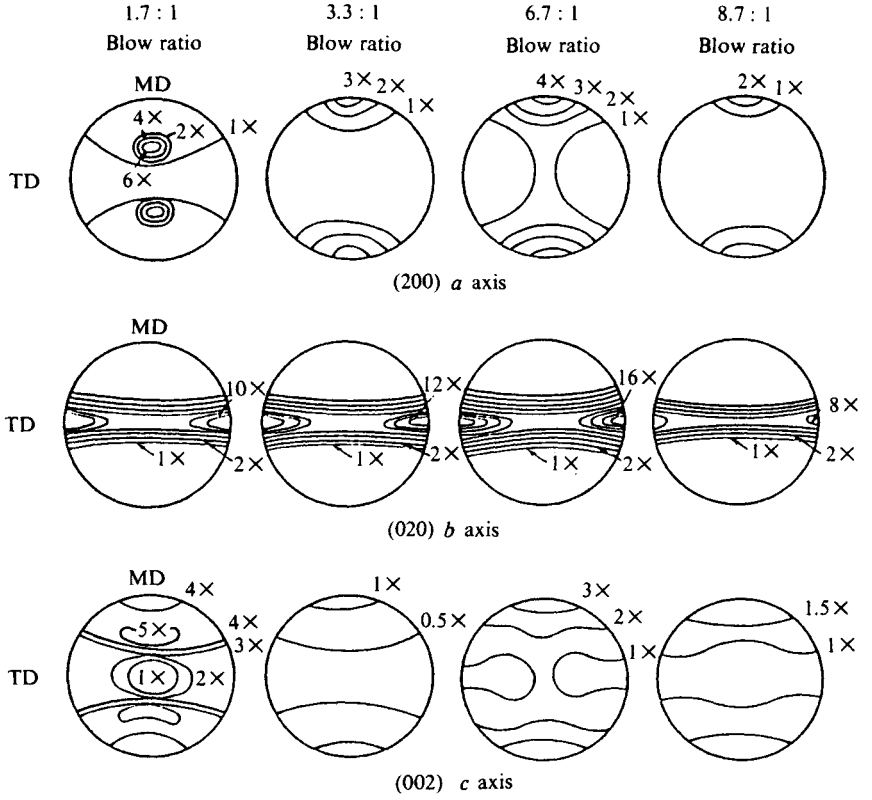

Fig. 10.16 Pole figures of extruded polyethylene film.[8)]
MD: Machine (rolling) direction.
TD: Transverse direction (parallel to rolled surface and normal to rolling direction)
[Reproduced with permission from P.H. Lindenmeyer, S. Lustig, *J. Appl. Polym. Sci.*, **9**, 235, John Wiley & Sons, Inc. (1965)]

is rather complex, but corresponding to the orientation of the *a* axis, the orientation distribution has maxima at angles of 45° and 135° to the plane of the film.

10.3 Determination of the Degree of Orientation

Specimens in which the crystallites exhibit the various types of orientation discussed hitherto can differ widely in the degree of the orientation. The reciprocal lattice point distribution bands are obviously affected by any spread in the orientations, and there is a corresponding effect on the X-ray diffraction patterns. The latter generally have an intensity distribution taking the form of arcs on Debye rings, but may (depending on the degree of orientation) vary from sharp points to uniform rings. The distribution of the reciprocal lattice points for a given crystal plane, *i.e.* the degree of orientation, can therefore be inferred from the intensity distribution of the corresponding diffraction on the Debye ring.

10.3.1 Criteria of the degree of orientation

A. Using meridional diffractions 00*l*

In a uniaxially oriented specimen, if the *a* and *b* axes of the crystallites are perpendicular to the *c* axis (fiber axis), δ_1 disappears for the 00*l* planes, *i.e.* the planes normal to the *c* axis, since $\varphi = 0$ and $\sigma = 0$ and hence $\cos \delta_m = \cos \delta_1 = 1/\cos \theta$. The 00*l* reciprocal lattice points should therefore lie on the *Z* axis, and since the diffraction sphere does not pass through the *Z* axis, no 00*l* diffractions should be observed. However, since the 00*l* reciprocal lattice points actually have a distribution $w(\varphi)$ they are distributed around the *Z* axis as well as on it. For low order numbers of *l*, therefore, the diffraction sphere cuts the distribution band of the reciprocal lattice points, and 00*l* diffractions are then produced (Fig. 10.17). Since the diffraction intensity distribution corresponds to the distribution $w(\varphi)$ of the reciprocal lattice points, it can be used directly to find the distribution of orientation. However, the 00*l* diffraction intensity distribution corresponds only to the flanks of the reciprocal lattice point distribution. In practice, therefore,

a) It is necessary to know the 00*l* intensity distribution from an inclination photograph for which the specimen was inclined at an angle of $\mu = \theta_{00l}$ (where θ_{00l} is the Bragg angle for the 00*l* diffractions) to the incident X-rays in order to be able to place the distribution band

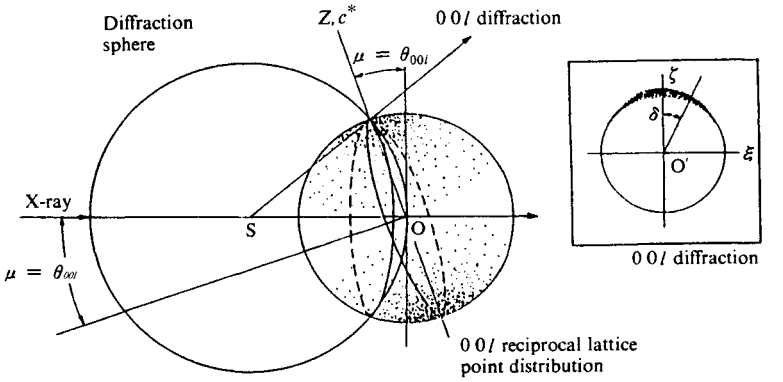

Fig. 10.17 Measurement of the degree of orientation using meridional diffractions.
Measurement of the meridional diffractions is possible when the specimen is inclined appropriately (see text).

of 00*l* reciprocal lattice points exactly on the diffraction sphere. Since this intensity distribution is along a small circle of the diffraction sphere, the following equation is used to convert it into a distribution along the great circle, and so to find the correct orientation distribution.

$$\cos\varphi = \cos\delta \cos\theta_{00l} \tag{10.12}$$

φ is the angle from the OZ axis, and δ is the angle from the meridian measured on the Debye ring (*cf.* Fig. 10.17).

b) Alternatively, the 00*l* diffraction intensity distribution can be found without the need for the correction (Eq. 10.12) required in *a)* above, by taking precession photographs of reciprocal lattice planes containing the c^* axis or from Weissenberg photographs for axes perpendicular to the c axis.†

B. A practical measure of parallelism[9]

If the degree of orientation is low, it is difficult to obtain pure meridian 00*l* diffraction intensity measurements. In such cases a practical measure of parallelism Π is found as follows from the intensity distribution of diffraction spots on the equator, and is used as a criterion of the degree of orientation. This quantity is defined by the equation

$$\Pi = \frac{180^\circ - H^\circ}{180^\circ} \times 100 \tag{10.13}$$

where H° is the half width of the intensity distribution on the Debye ring of the most intense diffraction on the equator. Π has a value of 0 if the specimen is completely unoriented, while if the crystallites are all arranged perfectly parallel to one another it is equal to 100.

10.3.2 Determination of the mean of the crystallite orientation distribution (orientation coefficient)

This method determines not the orientation distribution, but its mean value. The value obtained in this way should agree with the mean of the orientation distribution function described in Section 10.3.3, but the work and calculations are naturally less onerous than those involved in first determining the orientation distribution function and then its mean.

A. Uniaxial orientation[10]

If the Z axis is the fiber axis (Fig. 10.18) and the angles made by the a, b, and c axes of the crystallite with the Z axis are φ_a, φ_b, and φ_c, respectively, the orientation coefficients, F_a, F_b, and F_c†† representing the degrees of the three axes with respect to the Z axis are defined by the following equations.

$$\left.\begin{aligned} F_a &= (3\langle\cos^2\varphi_a\rangle - 1)/2 \\ F_b &= (3\langle\cos^2\varphi_b\rangle - 1)/2 \\ F_c &= (3\langle\cos^2\varphi_c\rangle - 1)/2 \end{aligned}\right\} \tag{10.14}$$

† The 00*l* diffraction is easily confused with the nearby 10*l* and 01*l* diffractions. These generally have small values of δ_1 and appear close to the meridian; they sometimes merge to give a single arc cutting the meridian. As the degree of orientation of the specimen increases, however, the intensity of the 00*l* diffraction spot decreases, whereas those of the 10*l* and 01*l* diffractions do not decrease but sometimes separate on either side of the meridian.

†† These F's are not to be confused with those (structure factors) in Sections 2.9, 4.2, 11.2, 11.4, etc.

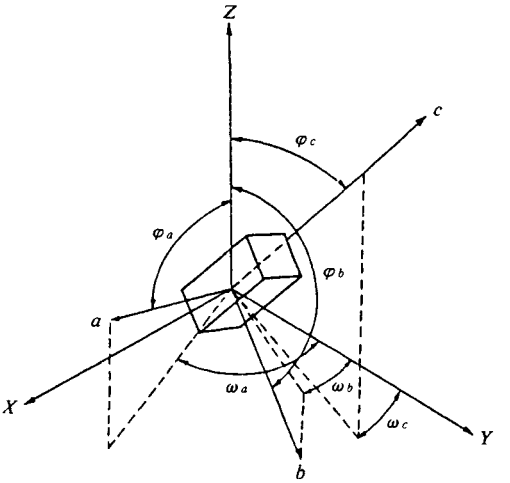

Fig. 10.18 Parameters used in the description of uniaxial crystallite orientation. [Reproduced from R.S. Stein, *J. Polym. Sci.*, **31**, 327, John Wiley & Sons, Inc. (1958)]

The values of $<\cos^2\varphi_a>$, $<\cos^2\varphi_b>$, and $<\cos^2\varphi_c>$ required for the determination of the orientation coefficients are found as follows.

If we consider, say, the orientation coefficient for the a axis, we have $\cos\varphi_a = \cos\theta_{h00}\sin\psi_{h00}$, with the mean given by

$$<\cos^2\varphi_a> = \cos^2\theta_{h00} <\sin^2\psi_{h00}>$$

$<\sin^2\psi_{h00}>$ is in turn given by

$$<\sin^2\psi_{h00}> = \frac{\int_0^{\pi/2} I(\psi_{h00})\sin^2\psi_{h00}\cos\psi_{h00}\mathrm{d}\psi_{h00}}{\int_0^{\pi/2} I(\psi_{h00})\cos\psi_{h00}\mathrm{d}\psi_{h00}}$$

Hence

$$<\cos^2\varphi_a> = \frac{\int_0^{\pi/2} I(\psi_{h00})\sin^2\psi_{h00}\cos\psi_{h00}\cos^2\theta_{h00}\mathrm{d}\psi_{h00}}{\int_0^{\pi/2} I(\psi_{h00})\cos\psi_{h00}\mathrm{d}\psi_{h00}} \tag{10.15a}$$

Similarly, for the b and c axes

$$<\cos^2\varphi_b> = \frac{\int_0^{\pi/2} I(\psi_{0k0})\sin^2\psi_{0k0}\cos\psi_{0k0}\cos^2\theta_{0k0}\mathrm{d}\psi_{0k0}}{\int_0^{\pi/2} I(\psi_{0k0})\cos\psi_{0k0}\mathrm{d}\psi_{0k0}} \tag{10.15b}$$

$$<\cos^2\varphi_c> = \frac{\int_0^{\pi/2} I(\psi_{00l})\sin^2\psi_{00l}\cos\psi_{00l}\cos^2\theta_{00l}\mathrm{d}\psi_{00l}}{\int_0^{\pi/2} I(\psi_{00l})\cos\psi_{00l}\mathrm{d}\psi_{00l}} \tag{10.15c}$$

$I(\psi_{h00})$, $I(\psi_{0k0})$, and $I(\psi_{00l})$ are the intensity distributions of the $h00$, $0k0$, and $00l$ diffractions on the Debye-Scherrer rings, and θ_{h00}, θ_{0k0}, and θ_{00l} are the measured values of the Bragg

angle for the $h00$, $0k0$, and $00l$ diffractions. ψ ($= 90° - \delta$) is the angle from the equator, measured on the Debye-Scherrer ring (Fig. 10.19).

In the special case where the a, b, and c axes of the crystallites are orthogonal, then

$$\cos^2 \varphi_a + \cos^2 \varphi_b + \cos^2 \varphi_c = 1 \tag{10.16}$$

$$F_a + F_b + F_c = 0 \tag{10.17}$$

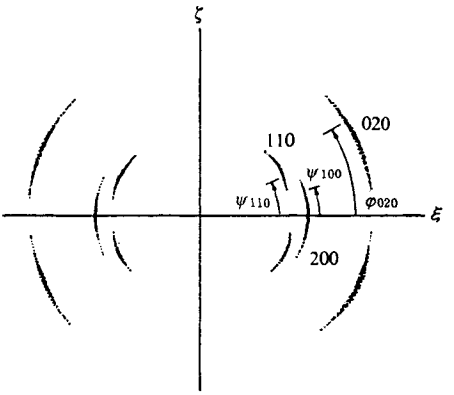

Fig. 10.19 Sketch of an X-ray diffraction pattern from oriented polyethylene.
The a axes are oriented perpendicular to the drawing direction. The degree of orientation is indicated by the intensity distributions along the diffraction arcs (*i.e.* the variation with φ).

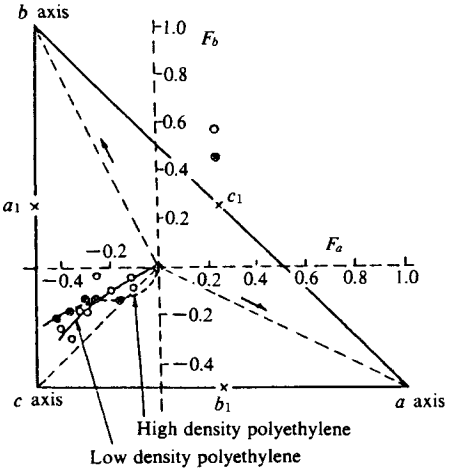

Fig. 10.20 Orientation diagram for polyethylene showing the effects of cold drawing.[11]
The orthogonal dotted lines are the axes of F_a and F_b and the origin corresponds to the unoriented state. Circles indicate low density polyethylene, and crosses indicate high density polyethylene.
[Experimental data supplied by R.S. Stein in private communication (1958)]

so that we need only determine the values of any two of the orientation coefficients.

Orientation coefficients of polyethylene.[10] Polyethylene belongs to the orthorhombic system (see Section 11.2.8), so Eq. 10.16 and 10.17 are normally valid. For spiral orientation as represented schematically in Fig. 10.19, F_a and F_b can be found by measuring the 200 and 020 intensity distributions $I(\psi_{200})$ and $I(\psi_{020})$ and calculating $<\cos^2\varphi_a>$ and $<\cos^2\varphi_b>$ from Eq. 10.15a and 15b. Fig. 10.20[11] shows how the orientation coefficients found in this way depend upon the conditions of cold drawing.

B. Biaxial orientation[12]

If the Z axis is the direction of the fiber axis and the Y axis lies in the plane of the film, the X axis is normal to the plane of the film. Two of the angles φ_a, φ_b, and φ_c used in the case of uniaxial orientation and any one of the angles ω_a, ω_b, and ω_c between the Y axis and the projections of the a, b, and c axis of the crystallite on the XY plane are required to define the orientation of the crystallites in the film specimen (*cf.* Fig. 10.18). The biaxial orientation coefficients F_{2a}, F_{2b}, and F_{2c} corresponding to the three angles just defined are given by the following equations.

$$\left.\begin{aligned} F_{2a}&=(3<\cos^2\omega_a>-1)\\ F_{2b}&=(3<\cos^2\omega_b>-1)\\ F_{2c}&=(3<\cos^2\omega_c>-1)\end{aligned}\right\} \tag{10.18}$$

The coefficients F_{2a}, F_{2b}, and F_{2c} are not independent, but obey the following relationships:

$$\left.\begin{aligned} \sin^2\varphi_a\cos^2\omega_a+\sin^2\varphi_b\cos^2\omega_b+\sin^2\varphi_c\cos^2\omega_c&=1\\ \sin^2\varphi_a\sin^2\omega_a+\sin^2\varphi_b\sin^2\omega_b+\sin^2\varphi_c\sin^2\omega_c&=1\end{aligned}\right\} \tag{10.19}$$

Thus if F_a and F_b are found as in the case of uniaxial orientation, there is a further requirement for two of F_{2a}, F_{2b},and F_{2c}, before the degree of orientation can be expressed. In the special case where (say) the c axes are parallel to the Z axis, $F_c=1$ and $F_a=F_b=-1/2$, and since $F_{2b}=F_{2a}$, it is necessary only to find either F_{2b} or F_{2a}.

a) Calculation of biaxial orientation coefficients.

$I(\varphi_a,\mu)_{h00}$ or $I(\varphi_b,\mu)_{0k0}$ is found from the $h00$ or $0k0$ diffraction intensity $I(\psi_{h00},\mu)$ or $I(\psi_{0k0},\mu)$ measured as a function of the angle μ between the incident X-rays and the X axis, *i.e.* between the incident X-rays and the normal to the film plane. For example, $I(\varphi_a,\mu)_{h00}$ is easily found from the $h00$ diffractions using the relationship

$$\cos\varphi_a=\cos\theta_{h00}\sin\psi_{h00}$$

This $I(\varphi_a,\mu)_{h00}$ is then used in the calculation of $<\cos^2\omega_{a0}>$, and hence to find F_{2a} (see Fig. 10.21).

$$\omega_a=\omega_{a0}+\mu$$

$$<\cos^2\omega_{a0}>=$$

$$\frac{\int_0^{\pi/2} I(\varphi_a,\mu)_{h00}[(\sin^2\theta_{h00})/(\sin^2\varphi_a)+\{1-(2\sin^2\theta_{h00})/(\sin^2\varphi_a)\}\cos^2\mu]\mathrm{d}\mu}{\int_0^{\pi/2} I(\varphi_a,\mu)_{h00}\,\mathrm{d}\mu} \tag{10.20a}$$

Similarly, F_{2b} is calculated with the aid of $<\cos^2\omega_{b0}>$ from the $0k0$ diffraction

$$<\cos^2\omega_{b0}>=$$

$$\frac{\int_0^{\pi/2} I(\varphi_b,\mu)_{0k0}[(\sin^2\theta_{0k0})/(\sin^2\varphi_b)+\{1-(2\sin^2\theta_{0k0})/(\sin^2\varphi_b)\}\cos^2\mu]\mathrm{d}\mu}{\int_0^{\pi/2} I(\varphi_b,\mu)_{0k0}\mathrm{d}\mu} \tag{10.20b}$$

If the uniaxial orientation coefficients F_a and F_b are calculated as described in the previous section, we now have all the orientation coefficients F_a, F_b, F_{2a}, and F_{2b} generally required to express the degree of orientation in cases of biaxial orientation.

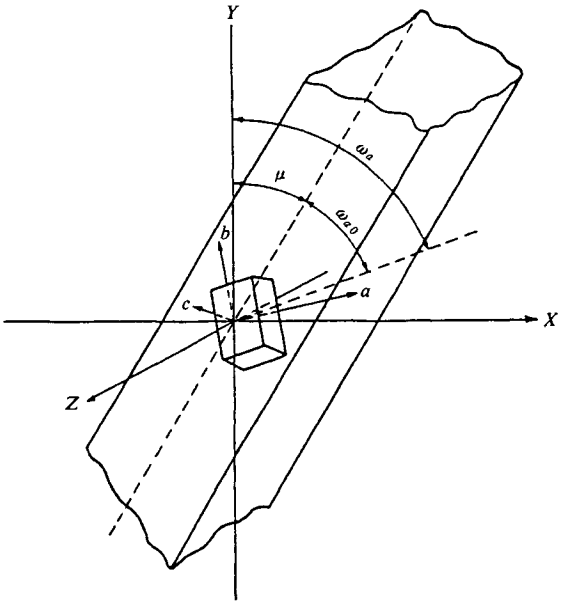

Fig. 10.21 Parameters used in the description of a tilted film.
[Reproduced from R.S. Stein, *J. Polym. Sci.*, **31**, 338, John Wiley & Sons, Inc. (1958)]

10.3.3 Analysis of the crystallite orientation distribution (orientation distribution functions)[13-15]

Crystallite orientation distributions are most suitably expressed in terms of crystallite orientation distribution functions. The calculations to determine these functions are rather laborious, and require high speed electronic computing facilities. The method has the compensating advantage, however, that the orientation distribution functions for planes giving very weak diffractions can be calculated from experimental results for many other planes.

A. Biaxial orientation distribution functions

The specimen is referred to the coordinate system O-*XYZ*, where the *Z* axis lies along the drawing direction, and the *YZ* plane is the plane of the specimen. The crystallites in the specimen have the coordinate system O-*xyz*, where the *x* direction is that of the molecular

chains. The orientation of the crystallites in the specimen is expressed by the Euler angles α, β, and γ (Fig. 10.22(a)). The reciprocal lattice vector $\boldsymbol{r}^*_j$, normal to a given crystal plane in a crystallite, can therefore be defined in terms of the angular parameters Θ_j and Φ_j in the coordinate system O-*xyz* of the crystallite (Fig. 10.22(b)) and in terms of χ_j and η_j in the coordinate system O-*XYZ* of the specimen (Fig. 10.22(c)). The two sets of angles (Θ_j, Φ_j) and (χ_j, η_j) are related by the formula

$$\begin{pmatrix} \sin\chi_j & \cos\eta_j \\ \sin\chi_j & \sin\eta_j \\ \cos\chi_j & \end{pmatrix} = T^{-1}(\alpha,\beta,\gamma) \begin{pmatrix} \sin\Theta_j & \cos\Phi_j \\ \sin\Theta_j & \sin\Phi_j \\ \cos\Theta_j & \end{pmatrix} \tag{10.21}$$

for changing from the O-*xyz* system to the O-*XYZ* system. In this formula,

$$T(\alpha,\beta,\gamma)=$$

$$\begin{pmatrix} \cos\alpha\cos\beta\cos\gamma-\sin\alpha\sin\gamma & \sin\alpha\cos\beta\cos\gamma+\cos\alpha\sin\gamma & -\sin\beta\cos\gamma \\ -\cos\alpha\cos\beta\sin\gamma-\sin\alpha\cos\gamma & -\sin\alpha\cos\beta\sin\gamma+\cos\alpha\sin\gamma & \sin\beta\sin\gamma \\ \cos\alpha\sin\beta & \sin\alpha\sin\beta & \cos\gamma \end{pmatrix} \tag{10.22}$$

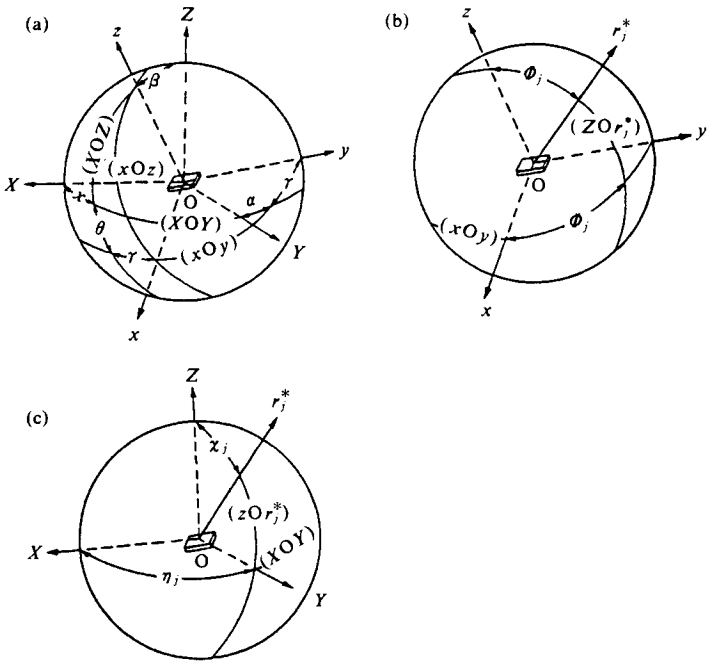

Fig. 10.22 Relationships between the coordinate systems and the reciprocal lattice vector $\boldsymbol{r}^*_j$.
(a) Specimen coordinate system, O-*XYZ*, and crystallite system, O-*xyz*, where α, β, γ are the Euler angles.
(b) Crystallite coordinate system and the arbitrary reciprocal lattice vector.
(c) Specimen coordinate system and reciprocal lattice vector $\boldsymbol{r}^*_j$.
[Reproduced with permission from R.-J. Roe, W. R. Krigbaum, *J. Chem. Phys.*, **40**, 2608, Am. Inst. Phys. (1964)]

With $\xi = \cos\beta$ and $\zeta_j = \cos\chi_j$, the crystallite orientation distribution function $w(\xi, \alpha, \gamma)$ may be expressed in terms of the experimental orientation distribution function $q_j(\zeta_j, \eta_j)$ for the reciprocal lattice vector $\boldsymbol{r}_j$ by means of the expanded forms of both $w(\xi, \alpha, \gamma)$ and $q_j(\zeta_j, \eta_j)$ which are obtained from the associated Legendre polynomials.[16] The expressions derived are of the following forms.

$$w(\xi,\alpha,\gamma)=\sum_{l=0}^{\infty}\sum_{m=-l}^{l}\sum_{n=-l}^{l}W_{lmn}Z_{lmn}(\xi)\exp(-im\alpha)\exp(-in\gamma) \tag{10.23}$$

$$q_j(\zeta_j,\eta_j)=\sum_{l=0}^{\infty}\sum_{m=-l}^{\infty}Q_{lm}{}^{j}P_l^m(\zeta_j)\exp(-im\eta_j) \tag{10.24}$$

$$Q_{lm}{}^{j}=2\pi\{2/(2l+1)\}^{1/2}\sum_{n=-l}^{l}W_{lmn}P_l^n(\Xi_j)\exp(-in\Phi_j) \tag{10.25}$$

$$\Xi=\cos\Theta$$

$P_l^m(\zeta)$ and $P_l^n(\Xi)$ are both normalized associated Legendre functions, while Z_{lmn} is a generalized associated Legendre function.[16] $w(\xi, \alpha, \gamma)$ is of course normalized.

The orientation distribution function $q_j(\zeta_j, \eta_j)$ for the reciprocal lattice vector $\boldsymbol{r}^*$ is found from the measured intensities $I(\zeta_j, \eta_j)$ for various independent lattice planes.

$$q_j(\zeta_j,\eta_j)=I(\zeta_j,\eta_j)/\int_0^{2\pi}\int_{-1}^{1}I(\zeta_j,\eta_j)\,\mathrm{d}\zeta_j d\eta_j \tag{10.26}$$

$Q_{lm}{}^{j}$ is then calculated from the following equation.

$$Q_{lm}{}^{j}=\frac{1}{2\pi}\int_0^{2\pi}\int_{-1}^{1}q_j(\zeta_j,\eta_j)P_l^m(\zeta_j)\exp(im\eta_j)\,\mathrm{d}\zeta_j d\eta_j \tag{10.27}$$

Having found the value of a given $Q_{lm}{}^{j}$ from Eq. 10.27, we find W_{lmn} ($n = -1,...,0,...,1$) for certain fixed values of l, m, and j with the aid of Eq. 10.25 by solving $(2l + 1)$ simultaneous first-order equations in the complex plane. If the number of $q_j(\zeta_j, \eta_j)$ obtained from experimental values is N, then W_{lmn} is found for at least $(N - 1)/2$ values of l. Finally, $w(\xi, \alpha, \gamma)$ can be calculated from Eq. 10.23.

It is convenient in practical calculations to express W_{lmn} and $Q_{lm}{}^{j}$ as

$$W_{lmn}=A_{lmn}+iB_{lmn} \tag{10.28}$$

$$Q_{lm}{}^{j}=a_{lm}{}^{j}+b_{lm}{}^{j} \tag{10.29}$$

Then

$$q_j(\zeta_j,\eta_j)=\sum_{l=0}^{\infty}\sum_{m=-l}^{l}P_l^m(\zeta_j)[a_{lm}{}^{j}\cos m\eta_j+b_{lm}{}^{j}\sin m\eta_j] \tag{10.30}$$

$$w(\xi,a,\gamma)=\sum_{l=0}^{\infty}\sum_{m=-l}^{l}\sum_{n=-l}^{l}Z_{lm}(\xi)[A_{lmn}\cos(m\alpha+n\gamma)+B_{lmn}\sin(m\alpha+n\gamma)] \tag{10.31}$$

$$\left.\begin{aligned} a_{lm}{}^{j} &= 2\pi\left\{\frac{2}{2l+1}\right\}^{1/2}\sum_{n=-l}^{l} P_l^n(\Xi_j)[A_{lmn}\cos n\Phi_j - B_{lmn}\sin n\Phi_j] \\ b_{lm}{}^{j} &= 2\pi\left\{\frac{2}{2l+1}\right\}^{1/2}\sum_{n=-l}^{l} P_l^n(\Xi_j)[A_{lmn}\sin n\Phi_j - B_{lmn}\cos n\Phi_j] \end{aligned}\right\} \tag{10.32}$$

Moreover, from the symmetry of Z_{lmn} and P_l^m, we obtain

$$\left.\begin{aligned} Q_{lm} &= (-1)^m Q_{l\bar{m}}{}^* \\ a_{lm} &= (-1)^m a_{l\bar{m}} \\ b_{lm} &= (-1)^{m+1} b_{l\bar{m}} \end{aligned}\right\} \tag{10.33}$$

$$\left.\begin{aligned} W_{lmn} &= (-1)^{m+n} W_{lm\bar{n}}{}^* \\ A_{lm} &= (-1)^{m+n} A_{lm\bar{n}} \\ B_{lm} &= (-1)^{m+n+1} B_{lmn} \end{aligned}\right\} \tag{10.34}$$

If the statistical distribution of the crystallites in the specimen has a certain symmetry, and if the crystallites themselves possess crystallographic symmetry elements, many of the W_{lmn} become zero, as shown in Tables 10.2 and 10.3,[15] with corresponding simplification of the calculation. The coordinate systems O-*xyz* and O-*XYZ* should therefore be chosen in such a way as to give the greatest possible number of symmetry elements.

When the crystallite coordinate system is changed to O-$\acute{x}\acute{y}\acute{z}$ by rotation of the O-*xyz* coordinate system through the Euler angles α', β', and γ' in order to manifest the highest degree of symmetry possible, the equation for the change of coordinates is

Table 10.2 Symmetry properties of Q_{lm} and W_{lmn} due to statistical symmetry of crystallite distribution

Statistical symmetry element	$q(\zeta, \eta)$	Q_{lm}	W_{lmn}
Mirror plane normal to x axis	$= q(\zeta, \pi - \eta)$	$= Q_{l\bar{m}}$	$= W_{l\bar{m}n} = (-1)^{m+n} W^*{}_{lm\bar{n}}$
Mirror plane normal to y axis	$= q(\zeta, -\eta)$	$= (-1)^m Q_{l\bar{m}}$	$(-1)^m W_{l\bar{m}n} = (-1)^n W^*{}_{lm\bar{n}}$
Mirror plane normal to z axis	$= q(-\zeta, \eta)$	$\begin{cases} \neq 0 \ (m \text{ even}) \\ = 0 \ (m \text{ odd}) \end{cases}$	$\begin{cases} \neq 0 \ (m \text{ even}) \\ = 0 \ (m \text{ odd}) \end{cases}$
Three mirror planes normal to x, y, and z axes respectively		$\begin{cases} = Q_{l\bar{m}} (m \text{ even}) \\ = 0 \ (m \text{ odd}) \end{cases}$	$\begin{cases} = W_{l\bar{m}n} = (-1)^n W^*{}_{lm\bar{n}} (m \text{ even}) \\ = 0 \qquad\qquad (m \text{ odd}) \end{cases}$
Cylindrical symmetry about z axis	$= q(\zeta, 0)$	$\begin{cases} \neq 0, m = 0 \\ = 0, m \neq 0 \end{cases}$	$\begin{cases} \neq 0, m = 0 \\ = 0, m \neq 0 \end{cases}$

[Reproduced with permission from R.-J. Roe, *J. Appl. Phys.*, **36**, 2024, Am. Inst. Phys. (1965)]

Table 10.3 Symmetry properties of W_{lmn} due to crystallographic symmetry of crystallites

Crystallographic symmetry element	Equivalent vectors of Θ and Φ	W_{lmn}
Mirror plane normal to X axis	$(\Theta, \pi - \Phi)$	$= (-1)^n W_{lm\bar{n}} = (-1)^m W^*{}_{l\bar{m}n}$
Mirror plane normal to Y axis	$(\Theta, -\Phi)$	$= W_{lm\bar{n}} (-1)^{m+n} W^*{}_{l\bar{m}n}$
Mirror plane normal to Z axis	$(\pi - \Theta, \Phi)$	$\begin{cases} \neq 0 \ (n \text{ even}) \\ = 0 \ (n \text{ odd}) \end{cases}$
r-fold rotational symmetry with respect to Z axis	$(\Theta, \Phi + 2\pi j/r)$ $(j = 1, 2, ..., r-1)$	$\begin{cases} \neq 0 \ (\text{if } n \text{ is a multiple of } r) \\ = 0 \ (\text{other cases}) \end{cases}$

[Reproduced with permission from R.-J. Roe, *J. Appl. Phys.*, **36**, 2024, Am. Inst. Phys. (1965)]

$$\begin{pmatrix} \sin\Theta_j & \cos\Phi_j \\ \sin\Theta_j & \sin\Phi_j \\ & \cos\Theta_j \end{pmatrix} = T^{-1}(\alpha',\beta',\gamma') \begin{pmatrix} \sin\Theta_j' & \cos\Phi_j' \\ \sin\Theta_j' & \sin\Phi_j' \\ & \cos\Theta_j' \end{pmatrix} \tag{10.35}$$

where Θ_j' and Φ_j' are the polar and azimuthal angles respectively of the reciprocal lattice vector $\boldsymbol{r}^*_j$ in the new coordinate system.

B. Uniaxial orientation distribution functions

For uniaxial orientation, $w(\xi, \alpha, \gamma)$ and qj(ζ_j, η_j) no longer contain the variables α and η_j; the orientation distribution functions and their interrelationships therefore reduce to the following.

$$w(\xi,\gamma) = \sum_{l=0}^{\infty} A_{l0} P_l^0(\xi) + \sum_{l=1}^{\infty} \sum_{m=1}^{l} [A_{lm} P_l^m(\xi) \cos m\gamma + B_{lm} P_l^m(\xi) \sin m\gamma)] \tag{10.36}$$

$$Q_l^j = 2\pi \left\{ \frac{2}{2l+1} \right\}^{1/2} \times \{A_{l0} P_l^0(\Xi_j) + 2 \sum_{m=1}^{l} (-1)^m [A_{lm} P_l^m(\Xi_j) \cos m\Phi_j + B_{lm} P_l^m(\Xi_j) \sin m\Phi_j]\] \tag{10.37}$$

Q_l^j is found from the experimental $q_j(\zeta_j)$ as follows.

$$Q_l^j = \int_{-1}^{1} q_j(\zeta_j) P_l(\zeta_j) d\zeta_j \tag{10.38}$$

$$q_j(\zeta_j) = I_j(\chi) / \int_0^{\pi} I_j(\chi) \sin\chi d\chi \tag{10.39}$$

C. Procedure for the calculation of $w(\xi, \gamma)$

1) The parameters Θ and Φ are calculated for the various diffractions from the size of the unit cell.

2) $I_j(\chi)$ is measured for the jth diffractions, and after correction for absorption, polarization, and Lorentz factors, $q_j(\zeta_j)$ is found from Eq. 10.39.

3) Eq. 10.38 is used to find the Q_l^j for $l = 0, 2, 4,...$ for the various diffractions. The expanded form of $q_j(\zeta_j)$ obtained with the aid of Q_l^j, *i.e.*

$$q_j(\zeta_j) = \sum_{l=0}^{\infty} Q_l^j P_l(\zeta_j) \tag{10.40}$$

is tested for convergence by means of Eq. 10.41, at the same time determining the number of terms of the associated Legendre polynomial required for convergence within the expected error, *i.e.* the minimum number of diffractions required to find the orientation distribution function with the expected accuracy.

$$\sigma_q^2 = \int_{-1}^{1} [q_j(\zeta_j)]^2 d\zeta_j - \sum_{l=0}^{\infty} (Q_l^j)^2 \tag{10.41}$$

4) The coefficients A_{lm} and B_{lm} required for the calculation of $w(\xi, \gamma)$ are found by applying Eq. 10.37 to each of the Q_l^j obtained and solving the simultaneous equations.

5) $w(\xi, \gamma)$ is calculated.

6) Where the orientation distribution function of a given crystal plane cannot be determined, *e.g.* because the diffraction intensity is too low, or because there is an unacceptable

amount of overlapping with other diffractions, the coefficients A_{lm} and B_{lm} used in the calculation of the orientation distribution functions of the crystal planes from other independent diffractions are used in Eq. 10.37 to calculate the required Q_l. If $q_j(\zeta_j)$ is then calculated from Eq. 10.40, $w(\xi, \gamma)$ can be calculated by the same procedure as for the other crystal planes.

7) When several superimposed diffractions are measured as one, the measured intensity must be broken down into the contributions due to the various components using the "weights" of the reciprocal lattice vectors $\boldsymbol{r}_j^*$. These weights C_{jp} are derived from the following equation.

$$C_{jp} = (F_{jp})^2 / \sum (F_{jp})^2 \tag{10.42}$$

F_{jp} is the structure factor of the reciprocal lattice vector $\boldsymbol{r}_{jp}^*$ measured as the reciprocal lattice vector $\boldsymbol{r}_j^*$ resulting from the superposition of other diffractions with very similar Bragg angles. We obtain

$$q_j(\zeta_j) = \sum_p C_{jp} q_{jp}(\zeta_j) \tag{10.43}$$

$$Q_l{}^j = \sum_p C_{jp} Q_l{}^{jp} \tag{10.44}$$

so that Eq. 10.37 is replaced by

$$Q_l{}^j = 2\pi \left\{ \frac{1}{2l+1} \right\}^{1/2} \{ A_{l0} \sum_p C_{jp} P_l{}^0(\Xi_j) + 2 \sum_{m=1}^{l} (-1)^m [A_{lm} \sum_p C_{jp} P_l{}^m(\Xi_j) \cos m\Phi_{jp} + B_{lm} \sum_p C_{jp} P_l{}^m(\Xi_j) \sin m\Phi_{jp}] \} \tag{10.45}$$

where $\Xi_{jp} = \cos\Theta_{jp}$.

Orientation distribution functions of drawn polyethylene.[14] Since poly-ethylene crystals are orthorhombic (*cf.* Section 11.2.7), the coordinate systems are chosen so that the x, y, and z axes coincide with the a, b, and c axes, respectively, of the unit cell. Owing to the presence of a mirror plane normal to the z axis, all the A_{lm} disappear from $w(\xi, \gamma)$ except those for which l and m are both even. Eqs. 10.36 and 10.45 thus become

$$w(\xi, \gamma) = \sum_{\substack{l=0 \\ (even)}}^{\infty} A_{l0} P_l{}^0(\xi) + 2 \sum_{\substack{l=2 \\ (even,\, even)}}^{\infty} \sum_{m=2}^{l} A_{lm} P_l{}^m(\xi) \cos m\gamma \tag{10.46}$$

$$Q_l{}^j = 2\pi \{ 2 / (2l+1) \}^{1/2} \{ A_{l0} \sum_p C_{jp} P_l{}^0(\Xi_{jp}) + 2 \sum_{\substack{m=2 \\ (even)}}^{l} A_{lm} \sum_p C_{jp} P_l{}^m(\Xi_j) \cos m\Phi_{jp} \} \tag{10.47}$$

The specimen in this case a sheet of polyethylene (Alathon-10) that had received 10 Mrad of radiation and was drawn (draw ratio 5.58 : 1) to induce uniaxial orientation. The intensity distributions $I(\chi)$ of 12 diffractions were measured, and the $q(\zeta)$ were calculated. Fig. 10.23 shows the $q(\zeta)$ for the four diffractions with the smallest angles. The circles are the experimental values, and the solid curves indicate the values found from the expanded approximation obtained from Eq. 10.40 with $l = 16$. The dashes give curves obtained by expanding the intensity distribution curves of the 12 diffractions (isolated from the 23 overlapping diffractions of Table 10.4) into a series and applying corrections so as to minimize the differences from all the experimental curves. The dotted curve shown in the 200 dia-

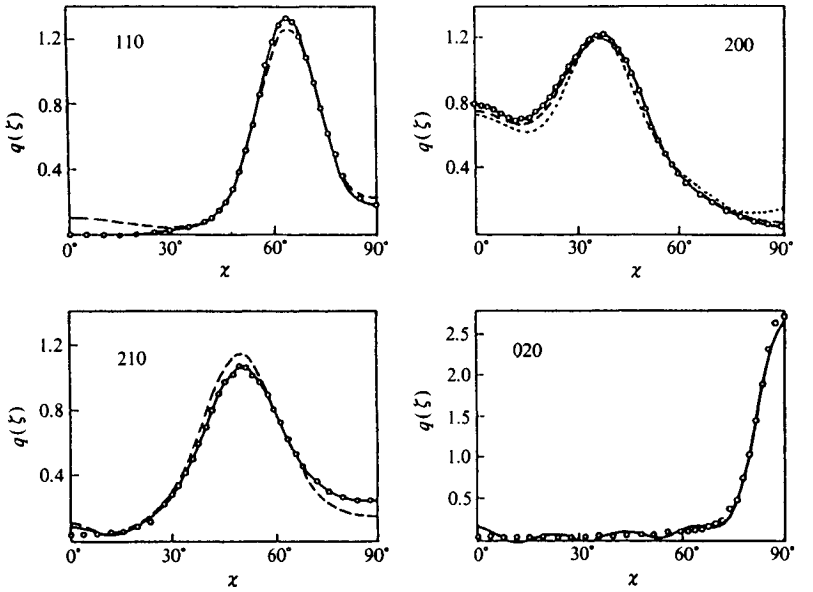

Fig. 10.23 Reciprocal lattice point distribution functions $q(\zeta)$ of the first four diffractions for uniaxially oriented polyethylene (see text).[14]
[Reproduced with permission from R.-J. Roe, W. R. Krigbaum, *J. Chem. Phys.*, **41**, 737, Am. Inst. Phys. (1964)]

Table 10.4 Identification of the diffractions, etc. for Fig. 10.23[14]

j	2θ, diffraction angle[deg]	ρ_j†	hkl	C_{jp}
1	21.62	1.0	110	
2	24.02	1.0	200	
3	30.15	1.0	210	
4	36.38	1.5	020	
5	39.79	0.7	011	0.81
			310	0.19
6	40.85	0.7	310	0.55
			011	0.30
			111	0.15
7	41.69	0.7	111	0.70
			310	0.19
			201	0.11
8	43.07	0.7	201	0.71
			220	0.15
			111	0.14
9	47.01	0.5	211	
10	55.00	0.5	311	0.88
			130	0.12
11	57.32	0.5	130	0.66
			221	0.34
12	61.92	0.5	401	0.60
			230	0.36
			420	0.04

† Weight due to superposition of diffractions.
[Reproduced with permission from W.R. Krigbaum, R.-J. Roe., *J. Chem. Phys.*, **41**, 737, Am. Inst. Phys. (1964)]

gram is the $q(\zeta)$ obtained from the intensity distribution curves of diffractions other than the 200 diffraction, using Eq. 10.47 and 10.40. Fig. 10.24 shows the resulting orientation distribution functions in the form of $G(\xi, \gamma) = 4\pi w(\xi, \gamma)$ instead of $w(\xi, \gamma)$. As the number of terms in the expanded approximation increases ($l = 6$, 12, 16), the approximation is improved and the negative regions decrease.

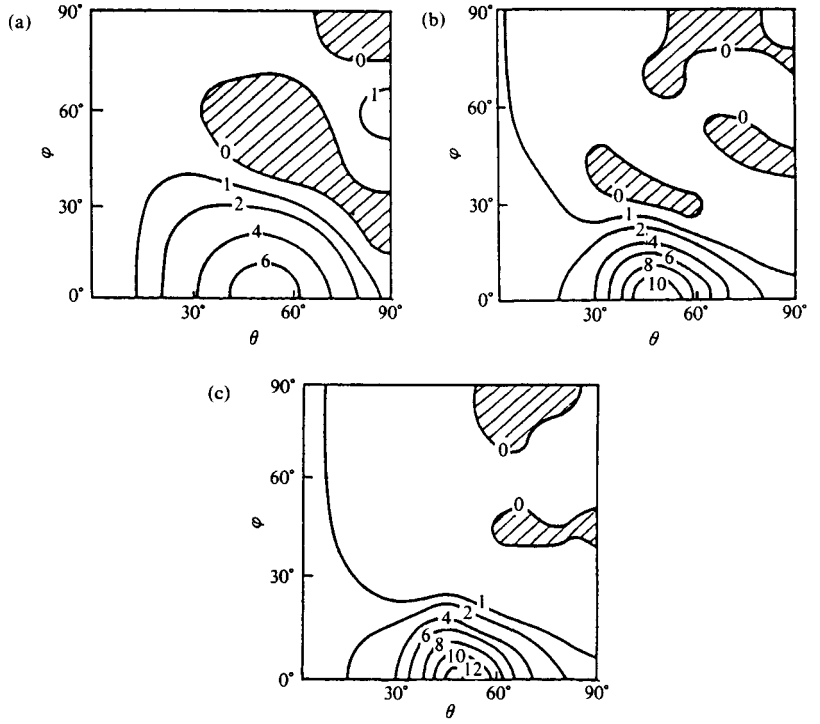

Fig. 10.24 Orientation distribution functions $G(\xi, \gamma) = 4w(\xi, \gamma)$.[14]
The number of terms used in the expanded approximation for (a), (b), and (c) were $l = 6$, 12, and 16, respectively. As the number of terms is reduced, the negative (shaded) area due to the approximation error increases.
[Reproduced with permission from W.R. Krigbaum, R.-J. Roe., *J. Chem. Phys.*, **41**, 737, Am. Inst. Phys. (1964)]

10.4 Preferred Orientation of Two-dimensional Lattices

In the previous sections the orientation of three-dimensional lattices has been discussed. The diffraction intensity of a two-dimensional lattice is represented in reciprocal space by a periodic array of parallel rod-like intensity distributions. The asymmetric interference lines produced by a randomly oriented two-dimensional lattice were discussed by Laue[17] and later by many other authors. The effect of non-random distribution of the two-dimensional lattices has been treated by Guentert and Cviekevich,[18] and has been generalized by Ruland and Tompa.[19] Ruland and coworkers also interpreted the effect of preferred orientation on (*hk*) interferences as shown by electron diffraction of carbon fibers.[20] Orientation of polymer chains (one-dimensional cases) will be dealt with in Section 14.5 (refer also 14.4 and 14.6).

References

1. T. Ishikawa, A. Sugihara, S. Nagai, N. Kasai, *J. Chem. Soc. Jpn.*, p.102, Chem. Soc. Jpn. (1978) (in Japanese).
2. T. Imura, in: *X-Ray Diffraction* (K. Kohra ed.), p. 600, Kyoritsu, Tokyo (1988) (in Japanese).
3. C.W. Bunn, *Chemical Crystallography*, 2nd ed., p. 192, Oxford University Press, London (1961).
4. R.W. James, *Optical Principles of the Diffraction of X-Rays*, p. 606, Bell & Sons, London (1964).
5. *International Tables for X-Ray Crystallography*, Vol. III. p. 295. Kynoch Press. Birmingham (1962).
6. B.D. Cullity, *Elements of X-Ray Diffraction*, sect. 2–11, Addison-Wesley, Reading (1956).
7. Y. Fujiwara, *J. Appl. Polymer Sci.*, **4**, 10 (1960).
8. P.H. Lindenmeyer, S. Lustig, *J. Appl. Polymer Sci.*, **9**, 227 (1965).
9. Y. Go, T. Kubo, *J. Chem. Soc. Jpn., Ind. Chem. Sect.*, **39**, 929, Chem. Soc. Jpn. (1939) (in Japanese).
10. R.S. Stein, *J. Polymer Sci.*, **31**, 327 (1958).
11. R.S. Stein, *ONR Technical Report.*, Nonr. 2151 (00), NR 356–78 (1957).
12. In ref. 10, p. 335.
13. R.-J. Roe, W.R. Krigbaum, *J. Chem. Phys.*, **40**, 2608 (1964).
14. W.R. Krigbaum, R.-J. Roe, *J. Chem. Phys.*, **41**, 737 (1964).
15. R.-J. Roe, *J. Appl. Phys.*, **36**. 2024 (1965).
16. For example, H. Margenau, G.M. Murphy, *The Mathematics of Physics and Chemistry*, p. 272, van Nostrand, N.Y. (1943).
17. M. von Laue, *Z. Krisl.*, **82**, 127 (1932).
18. O.J. Guentert, S. Cviekevich, *Carbon*, **1**, 309 (1964).
19. W. Ruland, H. Tompa, *Acta Cryst.*, **A24**, 93 (1968).
20. A. Fourdeux, R. Peret, W. Ruland, *J. Appl. Cryst.*, **1**, 252 (1968).